CHEMISTRY
A EUROPEAN JOURNAL

DOI: 10.1002/chem.200900167

Multiple Evidence for Gold(I)···Silver(I) Interactions in Solution

Eduardo J. Fernández,[a] Christopher Hardacre,[b] Antonio Laguna,[c] M. Cristina Lagunas,[b] José M. López-de-Luzuriaga,*[a] Miguel Monge,[a] Manuel Montiel,[a] M. Elena Olmos,[a] Raquel C. Puelles,[a] and Eva Sánchez-Forcada[a]

Abstract: $[AuAg_3(C_6F_5)(CF_3CO_2)_3(CH_2PPh_3)]_n$ (**2**) was prepared by reaction of $[Au(C_6F_5)(CH_2PPh_3)]$ (**1**) and $[Ag(CF_3CO_2)]$ (1:3). The crystal structures of complexes **1** and **2** were determined by X-ray diffraction, and the latter shows a polymeric 2D arrangement built by Au···Ag, Ag···Ag, and Ag···O contacts. The metallophilic interactions observed in **2** in the solid state seem to be preserved in concentrated THF solutions, as suggested by EXAFS, pulsed-gradient spin-echo NMR, and photophysical studies, which showed that the structural motif $[AuAg_3(C_6F_5)(CF_3CO_2)_3(CH_2PPh_3)]$ is maintained under such conditions. Time-dependent DFT calculations agree with the experimental photophysical energies and suggest a metal-to-ligand charge-transfer phosphorescence process. Ab initio calculations give an estimated interaction energy of around 60 kJ mol^{-1} for each Au···Ag interaction.

Keywords: ab initio calculations · EXAFS spectroscopy · gold · metal–metal interactions · silver

Introduction

One of the main concepts in chemistry, perhaps the most important, is that of the chemical bond. This terminology includes combinations between open-shell species, known as covalent bonding, and between closed-shell species formed by gain and loss of electrons, known as ionic bonding, although the real situation in molecules is intermediate between these extreme cases. In addition to these, weaker attractions among molecules or elements that appear as consequence of dipole interactions are known as van der Waals forces and, under certain circumstances, hydrogen bonding. Although weak, these attractions are recognized to play a major role in the design of multidimensional materials that have new or enhanced optical, conducting, vapochromic, magnetic, or other properties.[1,2] Among these secondary interactions, those between closed-shell metal centers, such as d^8, s^2, or d^{10}, represent a wide group with its own identity.[3] In fact, it is now evident that many examples of such interactions exist, and their strengths are, in some cases, comparable to strong hydrogen bonds. That is particularly the case for gold, which has been studied extensively,[4–6] as well as for other elements such as Ag^I,[7] Cu^I,[8] Hg^{II},[9] Pt^{II},[10] Pd^{II},[11] Tl^I,[12] Pb^{II},[13] and combinations[14] thereof. The advent of crystal structure analysis for the determination of molecular structures in the 1960s demonstrated the tendency of these species to form aggregates, which in many cases determines the structures of the complexes and even their properties. Hundreds of publications on this topic confirmed these findings, and the theorists rationalized the attraction as a consequence of correlation effects strengthened by relativistic effects, which reach a maximum at gold.[3–6]

In the case of gold/heteronuclear systems, this effect is expected to be more important with neighboring metals in the periodic table, since they are more affected by relativistic effects than early transition metals. Nevertheless, the number of structurally characterized gold/late transition metal complexes is still very limited, particularly for copper[15] and silver.[16] Consequently, theoretical information on these in-

[a] Dr. E. J. Fernández, Dr. J. M. López-de-Luzuriaga, Dr. M. Monge, Dr. M. Montiel, Dr. M. E. Olmos, R. C. Puelles, E. Sánchez-Forcada
Departamento de Química, Universidad de La Rioja
Grupo de Síntesis Química de La Rioja, UA-CSIC
Complejo Científico-Tecnológico, 26004 Logroño (Spain)
Fax: (+34) 941299621
E-mail: josemaria.lopez@unirioja.es

[b] Prof. C. Hardacre, Dr. M. C. Lagunas
School of Chemistry and Chemical Engineering
Queen's University, Belfast, BT9 5AG (UK)

[c] Prof. A. Laguna
Departamento de Química Inorgánica
Instituto de Ciencia de Materiales de Aragón
Universidad de Zaragoza-CSIC, 50009-Zaragoza (Spain)

Supporting information for this article is available on the WWW under http://dx.doi.org/10.1002/chem.200900167.

WILEY InterScience DISCOVER SOMETHING GREAT
© 2009 Wiley-VCH Verlag GmbH & Co. KGaA, Weinheim

teractions is very limited, because such studies are usually carried out to complement information obtained experimentally.

Obviously, the most accessible and straightforward way to determine the presence of metal–metal interactions in complexes is single-crystal X-ray diffraction analysis, but in some cases is not easy to obtain single crystals, and some substances do not exist in the solid state. In some cases the interactions can be detected by Raman[17] or electronic absorption and emission spectroscopy.[18] Structural information in solution is also very important to gain insight into the properties of the complexes in the absence of crystal packing forces. Information gathered in solution can lead to significant developments in photochemistry, crystal engineering, and medicine.[19] However, emissive behavior often disappears in solution, and the assignment of the luminescence to specific transitions is not always unambiguous. Moreover, in the case of fluorescent or colored samples recording of Raman spectra is highly problematic and in many cases unfeasible.

In this respect, Fackler et al. recently reported a pulsed-gradient spin-echo (PGSE) NMR study[20] that showed evidence of stacking of gold(I)–mercury(II) complexes in solution, and Lagunas et al. reported EXAFS studies[21] on dinuclear gold complexes in solution. In the first case, the degree of aggregation was dependant on the gold precursor, and the results were consistent with the presence of aggregates of both two and three trinuclear units in solution derived from an infinite polymer in the solid state. The EXAFS studies proved the existence of gold–gold interactions in solutions of dinuclear complexes with bridging ligands, but they were not found in other cases in which unsupported solid-state interactions appeared. In many cases application of different and complementary techniques is needed to unambiguously determine the presence of such interactions in solution and propose a structure in this medium.

Here we report the use of multiple techniques to study solutions of the complex $[AuAg_3(C_6F_5)(CF_3CO_2)_3(CH_2PPh_3)]_n$ (**2**); NMR, EXAFS, and photophysical techniques were used to demonstrate the existence of a gold–silver aggregate in solution with associated properties, and a correlation was made with a theoretical study on the energies of the related interactions.

Results and Discussion

Synthesis and characterization: The reaction between $[Au(C_6F_5)(CH_2PPh_3)]$ (**1**) and $[Ag(CF_3CO_2)]$ (1:3) in dichloromethane leads to a product of formula $[AuAg_3(C_6F_5)(CF_3CO_2)_3(CH_2PPh_3)]_n$ (**2**; Scheme 1). It is an air-stable orange solid that behaves as a nonconductor in acetone. The same solid is always formed when the reaction is carried out with different molar ratios of the reagents. Its analytical and spectroscopic data agree with the proposed formulation. Thus, its IR spectrum in Nujol mull shows, among others, absorptions at 1640 (vs) and 1190 cm^{-1} (vs) due to the trifluoroacetate anion, at 1501 (s), 961 (s), and 790 cm^{-1} (s) arising from the AuC_6F_5 fragment, and at 580 cm^{-1}(w) characteristic of $\nu(Au–C_{ylide})$.[22] The presence of the ylide ligand is also confirmed in the ^1H NMR spectrum, which displays a doublet at 2.03 ppm for the methylene group and a multiplet between 8.00 and 7.65 ppm corresponding to the aromatic protons. In addition, its $^{31}P\{^1H\}$ NMR spectrum shows a singlet at 31.7 ppm for the phosphorus atom of the ylide ligand. Its ^{19}F NMR spectrum displays three resonances at −116.6 (m, F_o), −164.4 (t, F_p, $^3J(F_p,F_m)=18.4$ Hz), and −165.9 (m, F_m), due to the three types of fluorine atoms of the pentafluorophenyl groups, and a singlet at −74.6 ppm due to the trifluoroacetate anion. Finally, the mass spectra (ES) of **2** display peaks at *m*/*z* 773 and 750, corresponding to the fragments $[Ag_3(CF_3CO_2)_4]^-$ and $[Au(CH_2PPh_3)_2]^+$, respectively.

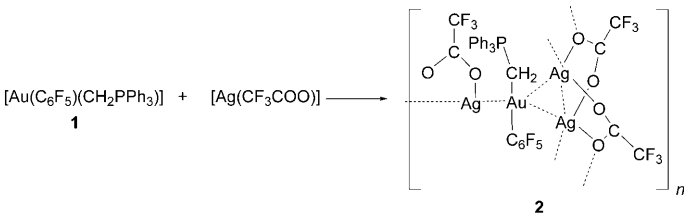

Scheme 1. Synthesis of complex **2**.

Crystal structures: The crystal structures of complexes **1** and **2** were determined by X-ray diffraction methods from single crystals obtained by slow diffusion of hexane into solutions of the complexes in dichloromethane. Experimental details, bond lengths, and bond angles are collected in Tables 1–3. Both complexes crystallize in triclinic space group $P\bar{1}$ with four and two formula units per unit cell, respectively. Thus, the crystal structure of **1** has two independent molecules of $[Au(C_6F_5)(CH_2PPh_3)]$ in the asymmetric unit (only one of them is shown in Figure 1), with the gold(I) centers in their usual linear environment by coordination to the *ipso*-C atom of a pentafluorophenyl group and to the methylenic C atom of an ylide ligand. The $Au–C_{aryl}$ bond lengths of 2.048(6) and 2.038(6) Å compare well with those observed in pentafluorophenylgold(I) ylides and methanides,[23] and lie in the middle of the range normally found in these complexes, that is 2.011(11)–2.086(82) Å. The $Au–C_{ylide}$ distances of 2.086(6) and 2.078(6) Å are similar to those observed in the crystal structures of $[Au(CH_2PPh_3)_2]A$ (2.087(5) and 2.077(5) Å for A = tetracyanoquinodimethanide; 2.088(3) and 2.079(3) Å for A = trifluoromethanesulfonate).[24] Although the $Au–C_{aryl}$ and $Au–C_{ylide}$ distances in **1** are similar, the former is slightly shorter than the latter, in accordance with the higher *trans* influence of aryl compared to ylide ligands. The shortest intermolecular Au···Au distance is longer than 5 Å and indicates the absence of aurophilic interactions between neighboring molecules.

Complex **2** crystallizes as a 2D polymer with a $[Au(C_6F_5)(CH_2PPh_3)]$ unit, a folded $[Ag_2(CF_3CO_2)_2]$ ring, and half of a second $[Ag_2(CF_3CO_2)_2]$ dimer in the asymmetric unit, con-

 © 2009 Wiley-VCH Verlag GmbH & Co. KGaA, Weinheim

Table 1. Data collection and structure refinement details for complexes **1** and **2**.

Compound	**1**	**2**
formula	$C_{25}H_{17}AuF_5P$	$C_{31}H_{17}Ag_3AuF_{14}O_6P$
crystal habit	colorless prism	colorless prism
crystal size [mm]	0.35×0.10×0.07	0.30×0.20×0.10
crystal system	triclinic	triclinic
space group	$P\bar{1}$	$P\bar{1}$
a [Å]	10.8753(7)	9.6270(10)
b [Å]	12.5777(7)	13.467(2)
c [Å]	17.4850(10)	15.770(3)
α [°]	71.332(3)	105.204(10)
β [°]	80.739(3)	95.138(10)
γ [°]	72.595(3)	96.763(10)
V [Å^3]	2156.5(2)	1943.70(5)
Z	4	2
ρ_{calcd} [g cm^{-3}]	1.972	2.226
M	640.32	1302.99
$F(000)$	1224	1224
T [°C]	−173	−100
$2\Theta_{max}$ [°]	54	54
$\mu(Mo_{K\alpha})$ [mm^{-1}]	6.949	5.399
reflns measured	27054	32386
unique reflns	9110	8174
R_{int}	0.0619	0.0391
R[a] ($I>2\sigma(I)$)	0.0414	0.0399
wR[b] (F^2, all reflns)	0.1081	0.1130
parameters	577	506
restraints	160	152
S[c]	0.994	1.044
$\Delta\rho_{max.}$ [e Å^{-3}]	3.320	2.728

[a] $R(F)=\Sigma||F_o|-|F_c||/\Sigma|F_o|$. [b] $wR(F^2)=[\Sigma\{w(F_o^2-F_c^2)^2\}/\Sigma\{w(F_o^2)^2\}]^{0.5}$; $w^{-1}=\sigma^2(F_o^2)+(aP)^2+bP$, where $P=[F_o^2+2F_c^2]/3$ and a and b are constants adjusted by the program. [c] $S=[\Sigma\{w(F_o^2-F_c^2)^2\}/(n-p)]^{0.5}$, where n is the number of data and p the number of parameters.

Table 2. Selected bond lengths [Å] and angles [°] for complex **1**.

Au1−C1	2.048(6)	Au2−C11	2.038(6)
Au1−C7	2.086(6)	Au2−C17	2.078(6)
C1-Au1-C7	179.7(2)		
C11-Au2-C17	177.7(2)		

Table 3. Selected bond lengths [Å] and angles [°] for complex **2**.[a]

Au−C1	2.060(7)	Ag1−O3	2.264(5)
Au−C10	2.088(6)	Ag1−O1	2.371(5)
Ag1−C1	2.641(7)	Ag1−O1$^{\#1}$	2.478(4)
Au−Ag1	2.8692(5)	Ag2−O4	2.230(6)
Au−Ag2	2.8846(6)	Ag2−O2	2.383(5)
Au−Ag3	2.9032(6)	Ag2−O2$^{\#2}$	2.366(4)
Ag1−Ag2	2.8842(7)	Ag3−O5	2.179(6)
Ag3−Ag3$^{\#3}$	2.9485(12)	Ag3−O6$^{\#3}$	2.180(6)
C1-Au-C10	174.3(3)	O4-Ag2-O2	126.6(2)
Ag1-Au-Ag2	60.167(15)	O4-Ag2-Au	97.21(18)
Ag1-Au-Ag3	133.454(18)	O2-Ag2-Au	114.41(12)
Ag2-Au-Ag3	128.75(2)	O5-Ag3-O6$^{\#3}$	160.4(2)
Au-Ag1-Ag2	60.182(15)	O5-Ag3-Au	114.47(15)
Ag1-Ag2-Au	59.651(14)	O6$^{\#3}$-Ag3-Au	84.21(14)
Au-Ag3-Ag3$^{\#3}$	164.42(4)	O5-Ag3-Ag3$^{\#3}$	80.33(15)
O3-Ag1-O1	110.85(19)	O6$^{\#3}$-Ag3-Ag3$^{\#3}$	80.61(14)
O3-Ag1-Au	104.06(14)	Au-Ag3-Ag3$^{\#3}$	164.42(4)
O1-Ag1-Au	125.08(11)		

[a] Symmetry transformations used to generate equivalent atoms: #1 $-x+1,-y,-z+1$; #2 $-x+2,-y,-z+1$; #3 $-x+2,-y+1,-z+1$.

nected through short Au···Ag contacts (Figure 2). An equivalent tetrametallic fragment is generated by an inversion center located at (1, 0.5, 0.5) leading to the formation of a nearly planar silver trifluoroacetate dimer in the center of the octametallic unit that runs parallel to the crystallographic x axis. This $[Ag_2(CF_3CO_2)_2]$ ring is nearly perpendicular to the other two dimers (Figure 3). The structure also expands along the y axis through Ag···O contacts between silver and oxygen atoms of adjacent bent $[Ag_2(CF_3CO_2)_2]$ rings, and thus in a two-dimensional polymeric structure results (Figure 3).

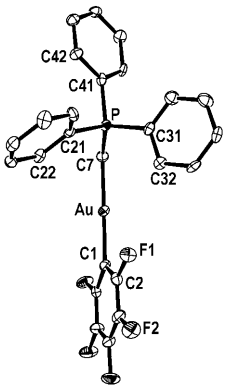

Figure 1. Molecular structure of complex **1** with atom labeling scheme. Hydrogen atoms have been omitted for clarity.

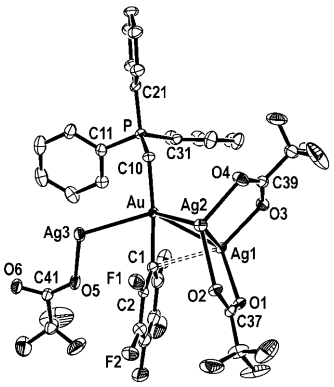

Figure 2. Asymmetric unit of the crystal structure of **2** (30% probability) with atom labeling scheme. Hydrogen atoms have been omitted for clarity.

Each gold center is bonded to three silver atoms with Au–Ag distances of 2.8692(5) and 2.8846(6) Å to the silver centers of the folded $[Ag_2(CF_3CO_2)_2]$ unit, forming a quasi-equilateral triangle, since the silver atoms of the ring also display an intermolecular metal–metal interaction of 2.8842(7) Å. Since gold is smaller than silver by approximately 0.07 Å,[25] it can be concluded that the Ag···Ag contact within the ring is stronger than the Au···Ag interactions, which is logical since the Ag···Ag interaction is doubly bridged by two trifluoroacetate groups. Similarly, as the Au···Ag1 contact is supported by an Ag···C interaction of 2.641(7) Å between Ag1 and the *ipso*-C atom of the aryl group, the Au···Ag1 distance (2.8692(5) Å) should be slightly shorter than the unsupported Au-Ag2 distance (2.8846(6) Å), as observed. The third Au···Ag interaction of 2.9032(6) Å, also unsupported, is even longer than the other two, but they all lie in the range 2.8135(5)–3.1347(7) Å found for the Au···Ag contacts in the related polymeric Au/Ag complexes $[AgAuR(CF_3CO_2)(tht)]_n$ (R = C_6F_5, C_6Cl_5;

 © 2009 Wiley-VCH Verlag GmbH & Co. KGaA, Weinheim

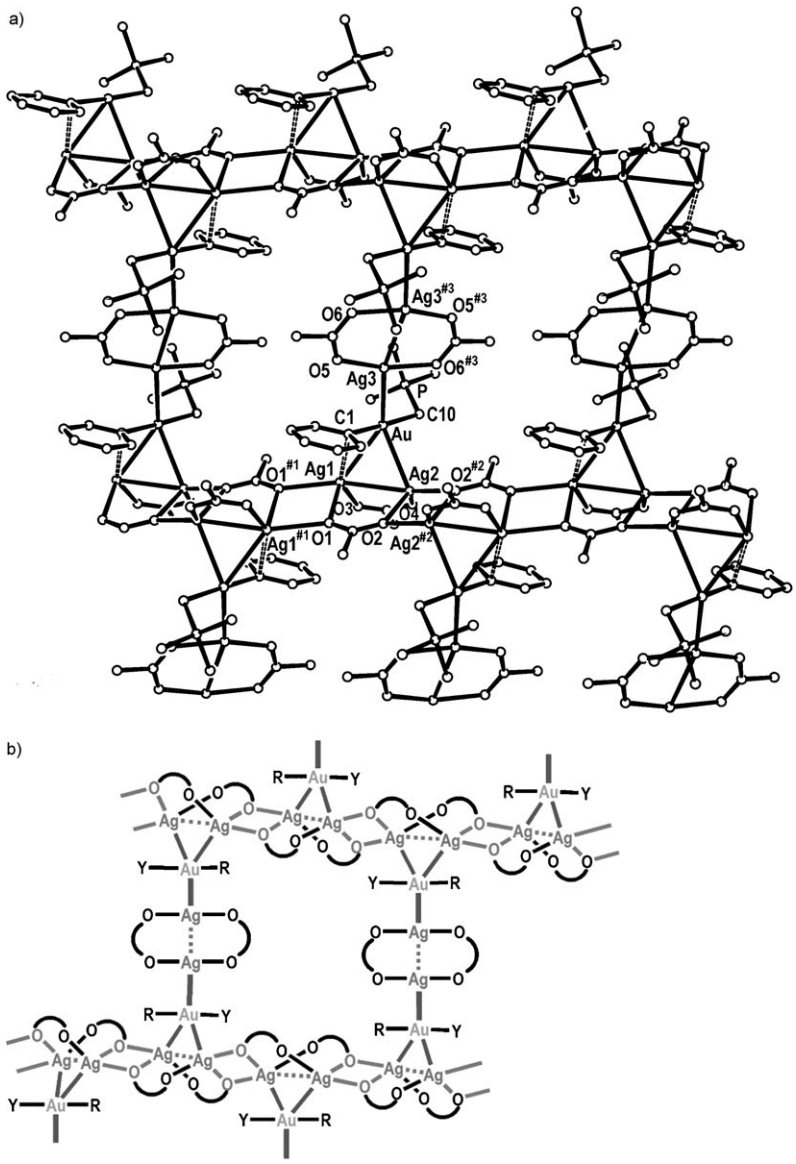

Figure 3. a) Two-dimensional structure of complex **2**. Hydrogen and fluorine atoms and phenyl groups in PPh_3 (except for the *ipso*-carbon atoms) have been omitted for clarity. b) Schematic of the polymeric structure of **2**. Au···Ag, Ag···Ag, and AgO···Ag contacts responsible for polymerization.

tht = tetrahydrothiophene), $[AuAg_2(C_6Cl_2F_3)(CF_3CO_2)_2(tht)]_n$,[16h] $[AuAg_4(mes)(RCO_2)_4(tht)_x]_n$ ($x=1$, $R=CF_3$, CF_2CF_3; $x=3$, $R=CF_2CF_3$; mes = mesityl, 2,4,6-$C_6Me_3H_2$), and $\{[AuAg_4(mes)(CF_3CO_2)_4(tht)(H_2O)]\cdot H_2O\cdot CH_2Cl_2\}_n$,[26] and is equal to the average Au···Ag distance in these species (2.9054 Å). The Ag···Ag contacts within the silver trifluoroacetate rings differ by about 0.06 Å, whereby the longest (2.9485(12) Å) corresponds to the planar dimer. This length is similar to the average of Ag···Ag distances observed in the related aryl gold(I)/silver perfluorocarboxylate derivatives described above[16h,26] (2.9609 Å), while the other (2.8842(7) Å) is shorter than most of the Ag···Ag lengths found in the same compounds, which lie in the range 2.8623(6)–3.0958(7) Å, and in most of the structures of complexes of the type $[Ag_2(RCO_2)_2L_n]$ ($n=1$, 2), which also display $(AgOCO)_2$ rings (2.8669(9)–3.3813(6) Å).[27]

The gold(I) center has the usual linear environment (if intermetallic contacts are not considered) with coordination to the *ipso*-C atom of the aryl group and to the carbon atom of the ylide with Au–C bond lengths of 2.060(7) and 2.088(6) Å, respectively, which compare well with those described for complex **1**. If the intermetallic interactions and the Ag···O contacts are considered, the silver centers of the folded ring (Ag1 and Ag2) display approximately trigonal-bipyramidal environments (see Table 3 and Figure 3), distorted as a consequence of the formation of an $AuAg_2$ triangle, with $O1^{\#1}$ and Ag2 or $O2^{\#2}$ and Ag1, respectively, in the apical positions. In contrast, Ag3 exhibits a distorted square-planar environment if metal–metal contacts are taken into account (Table 3). The Ag–O bond lengths in **2** vary from 2.179(6) to 2.383(5) Å, and thus they compare well with the range of Ag–O distances observed for the polymeric Au/Ag complexes cited above, which range from 2.151(3) to 2.488(6) Å. Thus, there are three pairs of Ag–O distances: 2.179(6) and 2.180(6) Å, 2.230(6) and 2.264(5) Å, and 2.371(5) and 2.383(5) Å. The shortest distances correspond to the planar silver trifluoroacetate dimers, in which all oxygen atoms act as terminal ligands and the silver center (Ag3) is "tetracoordinate"; the intermediate distances correspond to the Ag–O bonds between the silver centers of the folded dimers (with a higher coordination number) and the terminal oxygen atoms (O3 and O4); while the longest Ag–O bonds are those formed between the "pentacoordinate" silver atom and the bridging oxygen atoms (O1 and O2). The Ag–O distances between atoms of neighboring bent rings in the polymer would be expected to be similar to the latter since they are formed between "pentacoordinate" silver atoms and bridging oxygen atoms. However, there is only one with a similar length ($Ag2–O2^{\#2}$ 2.366(4) Å), with the second distance found to be longer

 © 2009 Wiley-VCH Verlag GmbH & Co. KGaA, Weinheim

(Ag1−O1$^{\#1}$ 2.478(4) Å). Such lengthening could be due to the additional interaction of Ag1 with the *ipso* carbon atom of the pentafluorophenyl group of 2.641(7) Å, which is longer than the Ag···C contacts present in the Au/Ag polymers mentioned above, in the range 2.362(6)–2.648(6) Å, with an average Ag−C distance of 2.526 Å.

EXAFS studies: Au L_{III} EXAFS spectra of $[AuAg_3(C_6F_5)(CF_3CO_2)_3(CH_2PPh_3)]_n$ (**2**) were collected in the solid state and in THF solution. The k^3-weighted EXAFS spectra and pseudoradial distribution functions are shown in Figure 4.

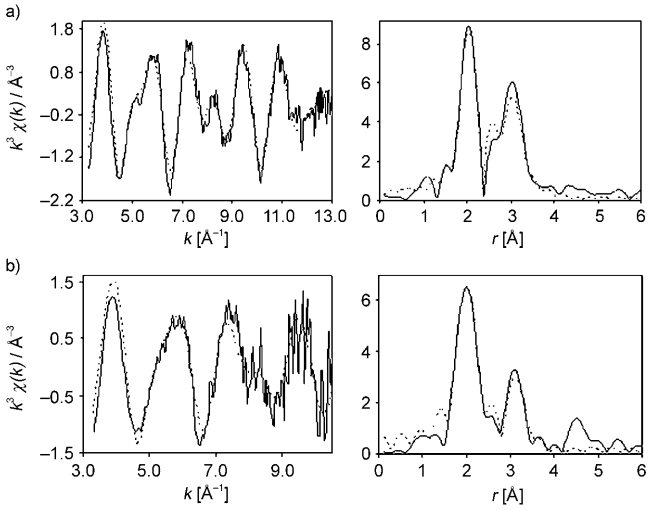

Figure 4. EXAFS and pseudoradial distribution functions (experimental: solid line; fitted: dotted line) for $[AuAg_3(C_6F_5)(CF_3CO_2)_3(CH_2PPh_3)]_n$ in the solid state (a) and dissolved in THF (b).

The interatomic distances determined by EXAFS are compared with those obtained from single-crystal X-ray diffraction studies in Table 4. These results show that the two Au−C and three Au···Ag distances obtained from the EXAFS data of the solid sample are in good agreement with the crystallographic data. For the dissolved compound, only the first three shells (i.e., two Au−C bonds and one Au···Ag interaction) could be modeled with confidence from the EXAFS data. The distances obtained were again in good agreement with those of the crystal structure. Further shells containing the other Ag atoms could not be fitted to the solution EXAFS data with any statistical significance. This is most likely due to the high level of noise of the solution data at $k > 10$ Å^{-1}. However, the similarity between the solid-state and solution EXAFS spectra and the fact that one Au···Ag contact is observed in solution suggest that the oligomeric structure of $[AuAg_3(C_6F_5)(CF_3CO_2)_3(CH_2PPh_3)]_n$ is maintained in solution to some extent. This agrees with observations by NMR spectroscopy, luminescence studies, and computations (see below).

Table 4. Selected parameters from the fitted EXAFS spectra of $[AuAg_3(C_6F_5)(CF_3CO_2)_3(CH_2PPh_3)]_n$ in the solid state and in solution in THF: Distances r between Au and neighboring atoms, Debye–Waller factors σ, and fit factors R^2. The number of atoms in each shell is one. Single-crystal X-ray crystallographic data is included for comparison, denoted as "crystal" in the table:

	Crystal r [Å]	Solid r [Å] (σ [Å^{-2}])	Solution r [Å] (σ [Å^{-2}])
C	2.059	2.04 (0.037)	1.99 (0.050)
C	2.088	2.08 (0.004)	2.05 (0.007)
Ag	2.869	2.78 (0.020)	2.79 (0.027)
Ag	2.885	2.86 (0.025)	–
Ag	2.903	3.05 (0.048)	–
		$R^2 = 27.3\%$	$R^2 = 39.3\%$

EXAFS studies were also performed for related complexes exhibiting extended Au···Ag interactions in their crystal structures, namely, $[AuAg_4(mes)(CF_3CO_2)_4(tht)]_n$, $[AuAg(C_6F_5)(CF_3CO_2)(tht)]_n$, and $[AuAg_2(C_6Cl_2F_3)(CF_3CO_2)_2(tht)]_n$ (see Supporting Information).[16h,26] In all cases, the EXAFS data indicated that the Au···Ag interactions were broken on dissolution, since only the [Au(aryl)(tht)] fragments could be observed in THF (in agreement also with luminescence studies previously reported).[16h] The exceptional robustness of $[AuAg_3(C_6F_5)(CF_3CO_2)_3(CH_2PPh_3)]_n$ may be attributed to the presence of an ylide ligand coordinated to Au instead of the more labile tht species. The better donor properties of the ylide would enhance the interaction energies.

PGSE NMR studies: ^{1}H pulsed-gradient spin-echo (PGSE) NMR experiments were carried out in $[D_8]$THF for different concentrations of compounds $[Au(C_6F_5)(CH_2PPh_3)]$ (**1**) or $[AuAg_3(C_6F_5)(CF_3CO_2)_3(CH_2PPh_3)]_n$ (**2**) (5–100 mM) with protiated tetrahydrofuran as internal standard (see Experimental Section and Supporting Information for details). This type of experiments allows the degree of aggregation between $[Au(C_6F_5)(CH_2PPh_3)]$ and $[Ag_2(CF_3CO_2)_2]$ fragments, which are the components of complex **2** in a 1:3/2 molar ratio, through Au^I···Ag^I interactions in solution to be evaluated.

With this methodology it is possible to measure the translational self-diffusion coefficient D_t for each compound and subsequently use the Stokes–Einstein equation to evaluate the molecular size through the hydrodynamic radius r_H. The D_t coefficients were determined by ^{1}H PGSE NMR analysis of the CH_2 doublet ylide resonances at 1.97 (**1**) and 2.03 ppm (**2**) (Figure 5).

Once the hydrodynamic radius is known, the molecular hydrodynamic volume V_H for each species in solution can be obtained. Table 5 lists the temperature and concentration used in each diffusion experiment, the diffusion coefficients D_t of **2** and the starting material **1** obtained under these conditions, and the calculated ratios between the hydrodynamic volumes of **2** and **1** in each case. This type of relationship between the hydrodynamic volume ratio of different molecular fragments was previously reported by Fackler and coworkers in a PGSE study on the aggregation between Au^I and Hg^{II} trinuclear fragments.[20]

The degree of aggregation has been estimated by the ratio $V_H^{(2)}/V_H^{(1)}$, where $V_H^{(2)}$ is the molecular hydrodynamic

© 2009 Wiley-VCH Verlag GmbH & Co. KGaA, Weinheim

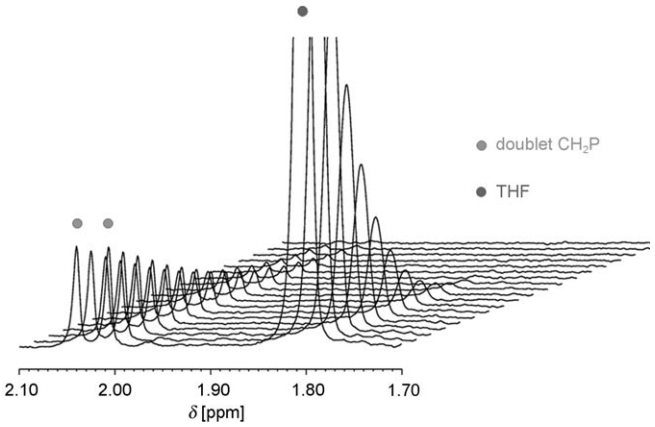

Figure 5. ^{1}H PGSE NMR spectra of **2** between $\delta = 1.70$ and 2.10 ppm in [D$_8$]THF. The resonance intensities of CH_2P and CH_2 (THF) protons decrease with increasing pulsed-field gradient. A faster decrease is observed in the case of the resonance intensity of CH_2 (THF) protons, because the smaller size of the solvent molecule leads to a larger self-diffusion coefficient D_t.

Table 5. PGSE results: diffusion coefficients for complexes $[AuAg_3(C_6F_5)(CF_3CO_2)_3(CH_2PPh_3)]_n$ (**2**) and $[Au(C_6F_5)(CH_2PPh_3)]$ (**1**) and hydrodynamic volume ratios under different experimental conditions.

c [mM]	T [K]	Species	D_t [10^{-10} m^{2}s^{-1}]	$V_H^{(2)}/V_H^{(1)}$
5	298	**2**	9.665	1.334
		1	10.710	
45	298	**2**	6.775	1.724
		1	8.692	
45	223	**2**	1.674	1.802
		1	2.079	
100	298	**2**	7.080	1.709
		1	8.477	

volume of **2**, and $V_H^{(1)}$ the molecular hydrodynamic volume of **1**. Thus, when $V_H^{(2)}/V_H^{(1)}$ is greater than 1, aggregation of $[Au(C_6F_5)(CH_2PPh_3)]$ and $[Ag_2(CF_3CO_2)_2]$ fragments through Au^I···Ag^I interactions can be proposed.

At room temperature, when the concentration of the sample is 5 mM, $V_H^{(2)}/V_H^{(1)}$ is slightly greater than unity (1.334). At a sample concentration of 45 mM, the calculated $V_H^{(2)}/V_H^{(1)}$ ratio is 1.724 at 298 K, and 1.802 at 223 K. The experimental PGSE value of $V_H^{(2)}/V_H^{(1)}$ at room temperature and 100 mM concentration is 1.709.

Conversely, the molecular volume of complexes $[AuAg_3(C_6F_5)(CF_3CO_2)_3(CH_2PPh_3)]_n$ (**2**) and $[Au(C_6F_5)(CH_2PPh_3)]$ (**1**) can be calculated from the X-ray data reported above by dividing the volume of the crystallographic cell by the number of molecules of each compound that are present in the unit cell. Thus, the measured volumes, $V_{X\text{-ray}}^{(2)} = 971.85$ and $V_{X\text{-ray}}^{(1)} = 539.125$ Å^3 lead to a $V_{X\text{-ray}}^{(2)}/V_{X\text{-ray}}^{(1)}$ ratio of 1.80. This ratio perfectly matches that obtained in PGSE experiments at 45 mM and 298 K or 223 K and at 100 mM and 298 K.

These results indicate that at concentrations from 45 to 100 mM, aggregation between $[Au(C_6F_5)(CH_2PPh_3)]$ and $[Ag_2(CF_3CO_2)_2]$ fragments is detected by PGSE experiments, and that this aggregation through Au^I···Ag^I interactions is very similar to that observed in the solid state by X-ray diffraction. In addition, decreasing the temperature to 223 K does not seem to significantly affect the degree of aggregation.

At lower concentrations (5 mM) at 298 K, the calculated $V_H^{(2)}/V_H^{(1)}$ ratio of 1.334 indicates loss of aggregation, although some Au^I···Ag^I metallophilic interactions could still be present in solution.

In conclusion, PGSE NMR experiments support the existence of Au···Ag interactions in solution, in agreement with the results obtained by EXAFS on 45 mM THF solutions, that is, the $AuAg_3$ stoichiometry is preserved in solution with the same or a different structure.

Photophysical properties: Both the precursor gold complex $[Au(C_6F_5)(CH_2PPh_3)]$ (**1**) and heteronuclear gold silver complex $[AuAg_3(C_6F_5)(CF_3CO_2)_3(CH_2PPh_3)]_n$ (**2**) show luminescence on irradiation with ultraviolet light.

The gold complex emits at 478 nm ($\lambda_{exc} = 357$ nm) in the solid state at 77 K, but it does not show luminescence at room temperature or in solution even at concentrations near saturation. In glassy EtOH/MeOH/CH_2Cl_2 (8/2/1) medium at 77 K this complex emits at 415 nm ($\lambda_{exc} =$ 286 nm).

The absorption spectrum of a solution (5×10^{-4} M) of this complex in degassed THF is characterized by two bands at 251 ($\varepsilon = 4300$ mol^{-1} dm^3 cm^{-1}) and 292 nm ($\varepsilon =$ 690 mol^{-1} dm^3 cm^{-1}), which increase with increasing concentration, without varying their positions. Therefore, aggregation in solution is not likely to occur even at higher concentrations (up to 45 mM). Time-dependent (TD) DFT calculations suggest that these absorptions are due to a mixture of ylide intraligand (IL) and metal-to-ligand (gold-to-ylide) charge-transfer (MLCT) transitions. Note that the orbital 123a (HOMO), which is formed mostly by orbitals of the pentafluorophenyl ring, is not involved significantly in these absorptions, and instead the ylide group acts as the source of the electronic transitions. This result differs from those obtained with anionic $[Au(C_6X_5)_2]^-$ or neutral $[Au(C_6F_5)(tht)]$ fragments, either by themselves[16h] or bonded to heterometals such as thallium, silver, and copper. In these, the pentafluorophenyl groups were in the origin of the electronic transitions.[16j,18]

Comparison between absorption and excitation spectra indicates that the transition responsible for luminescence is forbidden, since the maximum excitation energy is redshifted from the highest wavelength absorption band. This was confirmed by determination of the lifetime in the solid state at 77 K, which fits a biexponential decay with values of 28 and 5 μs ($R^2 = 0.999$), in accordance with a phosphorescence process. The TDDFT calculations on the first triplet absorption gave an energy of 344 nm, very close to the experimental excitation wavelength (357 nm). Analysis of the orbitals involved shows again a mixed intraligand (ylide) and metal-to-ligand (gold-to-ylide) charge-transfer transition, perhaps

 © 2009 Wiley-VCH Verlag GmbH & Co. KGaA, Weinheim

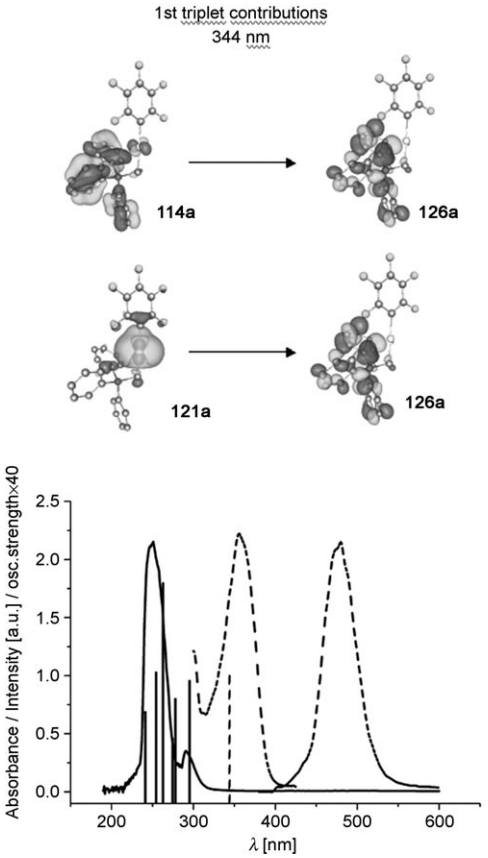

Figure 6. Most important contributions to the first triplet excitation (top). Absorption spectrum in 5×10^{-4} M THF solution (black line), excitation and emission profiles in the solid state at 77 K (dashed black lines), and first few singlet (black bar) and first triplet (dashed black bar) excitations calculated at the TDDFT level for complex **1** (bottom).

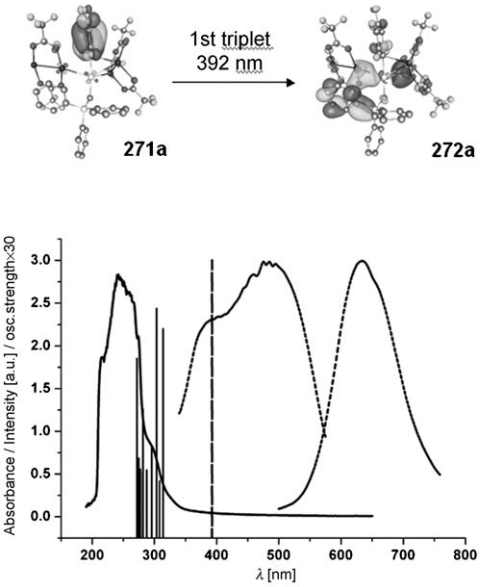

Figure 7. Most important contribution to the first triplet excitation (top). Absorption spectrum in 5×10^{-4} M THF solution (black line), excitation and emission profiles in the solid state at 77 K (dashed black line), and first few singlet (black bar) and first triplet (dashed black bar) excitations calculated at the TDDFT level for complex **2** (bottom).

the counterpart of the above-mentioned transition (Figure 6).

The optical behavior of the gold silver compound **2** is different to that of **1**. For instance, complex **2** shows luminescence in the solid state at room temperature ($\lambda_{em}=634$; $\lambda_{exc}=390$, 470) as well as at 77 K ($\lambda_{em}=658$ nm; $\lambda_{exc}=390$, 525 nm). Also, solutions of this complex in THF have absorption spectra that are concentration-dependent. Thus, on increasing the concentration from 5×10^{-4} to 5×10^{-3} and then to 45×10^{-3} M, a gradual redshift in the absorption edge was observed from about 250 to about 425 nm with a tail extending to about 600 nm and without external signs of saturation. These low absorption energies are consistent with the dark yellow color of complex **2** as a solid and in concentrated solutions. The shift of the absorption edge is indicative of molecular aggregation as the concentration is increased. This is consistent with the extended-chain structure observed for the solid.

Analysis of the theoretical absorption bands with the highest oscillator strengths obtained by TDDFT calculations on a model composed of the repeating unit that leads to the polymer suggests that those at higher energies (between 313 and 272 nm) consist of transitions from electron-rich pentafluorophenyl and trifluoroacetate ligands, with some contribution of gold–gold-, silver-, and ylide-based orbitals (see Figure 7). Therefore, they can be defined as mixtures of MLCT and LLCT. In this case the role of the perhalophenyl ring is conventional for this type of complexes, in contrast to that observed in the precursor ylide complex (see above).

The excitation spectrum is redshifted from these bands, and therefore they are not considered responsible for the luminescent behavior. It is likely that the transition that gives rise to the emission has a forbidden character. This is confirmed by lifetime measurements, which gave a biexponential decay of 14.3 and 2.7 μs ($R^2=0.998$) at room temperature. In this case, the theoretical calculations on the first triplet transition match one of the excitation maxima (392 and 390 nm, respectively) and show that the orbitals involved are the HOMO and LUMO. These are formed by the pentafluorophenyl ring with a small contribution of the metal atoms (HOMO), and the silver centers with a contribution of one of the phenyl rings of the ylide moiety (LUMO), respectively. Therefore, from this data, it can be proposed that the luminescent behavior found in this complex arises from a triplet ligand-to-metal charge transfer (^{3}LMCT) state (Figure 7).

Interestingly, this complex also shows luminescence in solution at similar concentration to those used in the PGSE and EXAFS studies, which suggests the existence of unsupported metal–metal interactions in solution. Thus, while 0.5 or 5 mM solutions do not exhibit detectable luminescence, at a concentration of 45 mM visible yellow-orange emission is

 © 2009 Wiley-VCH Verlag GmbH & Co. KGaA, Weinheim

observed when the solution is irradiated with UV/Vis light. In this case, the maximum emission appears at 570 nm on excitation at 390 nm. The longer wavelength found in the solid state (630 nm) compared to that in solution is likely due to the oligomeric nature of the complex in solution, instead of the infinite chain structure found in the solid. It has been reported that, as the number of interacting units increases, the emission shifts to lower energies.[18,28]

Finally, deviation from the Beer–Lambert law attributed to oligomerization has been reported for other interacting d^{10}–d^{10} centers.[29] Of these, the only report describing optical changes with concentration due to Au^I–Ag^I bonding was that of Omary, Fackler et al.,[29b] but the spectral changes referred only to the absorption spectrum because the product was not luminescent in solution. Hence, this represents the first example of luminescence in solution due to unsupported argento-aurophilic bonding.

Ab initio calculations: Ab initio calculations were carried out to gain insight into the nature of the metallophilic interactions found for complex **2**. Models **C1**–**C4** were built up as described in the Supporting Information. These model systems represent, in separate fragments, the possible molecular structure of complex **2**. For instance, models **C1** and **C2** are used to explain the interaction between $[Au(C_6F_5)(CH_2PPh_3)]$ and $[Ag(CF_3CO_2)]$ through only one Au···Ag interaction, whereas **C3** and **C4** are used to analyze the interaction between the same fragments through two Au···Ag interactions. Models **C1** and **C3** were obtained through full optimizations at DFT and MP2 levels of theory, respectively. In the case of model **C1** a theoretical local minimum displaying an Au···Ag and a C_{ipso}···Ag interaction is reached. Attempts to optimize model **C3** at the DFT level led to a local minimum in which Au···Ag and C_{ipso}···Ag interactions were not present at the same time and the dinuclear silver fragment was not bent outwards, while at the MP2 level both Au···Ag and C_{ipso}···Ag interactions are observed. Since the analysis of the Au···Ag interaction alone in model **C1** was not possible through a full optimization, a new model (**C2**) was proposed. Model **C2** was obtained by combination of the separately DFT optimized gold and silver fragments. Finally, model **C4** was obtained by displacement of the gold(I) fragment in model **C3** in order to avoid the Ag···C_{ipso} interactions and analyze only the two metallophilic Au···Ag interactions, in a similar way to that reported previously (Figure 8).[30]

To analyze the effects governing the aggregation of the $AuAg_3$ core due to interactions between one mononuclear gold fragment and two dinuclear silver fragments and to limit the computational cost, ab initio calculations were carried out at Hartree–Fock (HF) and second-order Møller–Plesset (MP2) levels of theory on models **C1**–**C4**, in separated $AuAg_2$ sub-fragments. The interaction energies (BSSE-corrected) between the gold and silver fragments were studied at different distances for models **C1**–**C4** (Figure 8). Thus, for each model, the stabilization produced by one Au···Ag and one Ag···C_{ipso} interaction (**C1**); one Au···Ag interaction

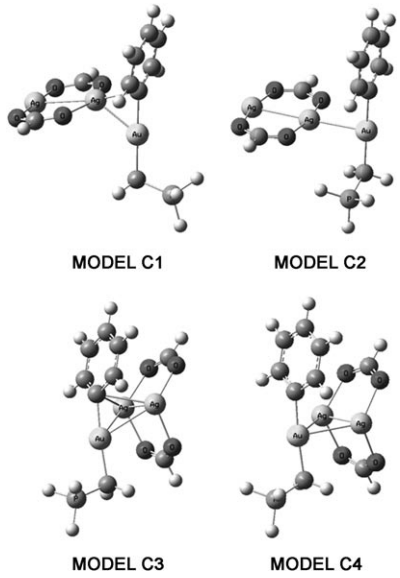

Figure 8. Theoretical model systems.

(**C2**); two Au···Ag and two Ag···C_{ipso} interactions (**C3**); or two Au···Ag interactions (**C4**) were studied. In this way the total interaction energy between $[Au(C_6H_5)(CH_2PH_3)]$ and $[Ag_2(CO_2H)_2]$ fragments can be estimated in the gas phase in all the possible structural dispositions observed experimentally, and the results can thus be compared with the molecular aggregation observed in solution.

In models **C1** and **C2**, the analysis of the interaction energy of $[Au(C_6H_5)(CH_2PH_3)]$ and $[Ag_2(CO_2H)_2]$ fragments at the MP2 (BSSE-corrected) level of theory leads to Au···Ag equilibrium distances of 2.86 and 2.81 Å, respectively, which are very close to the experimental value of 2.90 Å. In model **C1**, the presence of an extra Ag···C_{ipso} interaction (2.48 Å) together with the metallophilic Au···Ag one gives rise to a stabilization of $-98\ kJ\,mol^{-1}$, while in model **C2** the stabilization due to the Au···Ag interaction is $-61\ kJ\,mol^{-1}$. Since the experimental structure does not display any C_{ipso}···Ag contact for this fragment, it can be concluded that model **C2** represents fairly well this part of the structure and that the stabilization of $-61\ kJ\,mol^{-1}$ arises from the metallophilic Au···Ag interaction. The HF curve gives information on the ionic contribution to the intermolecular interactions, since correlation effects are not included at this theoretical level. In the case of model **C2** this ionic stabilization is slightly attractive at the equilibrium distance (ca. $-5\ kJ\,mol^{-1}$; Figure 9).

Models **C3** and **C4** permit the interaction energy between $[Au(C_6H_5)(CH_2PH_3)]$ and $[Ag_2(CO_2H)_2]$ fragments to be analyzed in the experimental structural arrangement in which two silver centers interact with a gold atom at the same time in the presence of one Ag···C_{ipso} interaction. Model **C3** shows two Au···Ag interactions and two Ag···C_{ipso} interactions, instead of one, for reasons of symmetry and computational feasibility. Model **C4** has just two Au···Ag interactions (see Figure 8).

 © 2009 Wiley-VCH Verlag GmbH & Co. KGaA, Weinheim

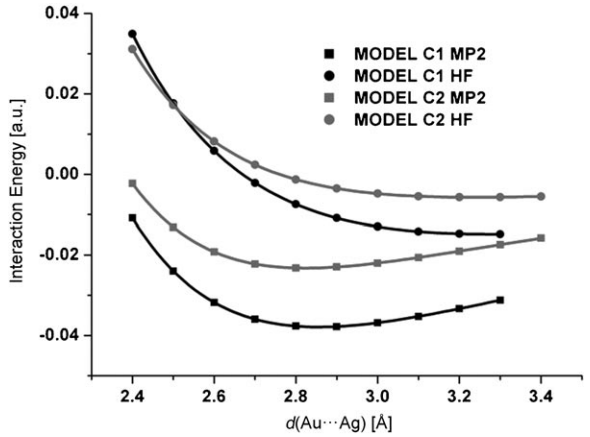

Figure 9. Interaction energies for the $[Au(C_6H_5)(CH_2PH_3)]\cdots[Ag_2(CO_2H)_2]$ interaction in models **C1** and **C2** at the HF and MP2 levels of theory.

Optimization of model **C3** at the MP2 level of theory and further BSSE correction for the interaction energies at different distances lead to Au···Ag and Ag···C_{ipso} equilibrium distances of 3.09 Å and 2.83 Å, respectively (Figure 10).

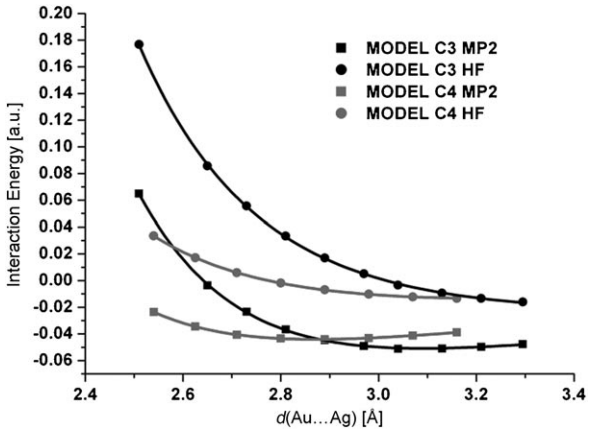

Figure 10. Interaction energies for the $[Au(C_6H_5)(CH_2PH_3)]\cdots[Ag_2(CO_2H)_2]$ interaction in models **C3** and **C4** at the HF and MP2 levels of theory.

These distances are slightly larger than the experimental ones of 2.87 and 2.64 Å, respectively, but the shape of the silver fragment, in which the O-Ag-O angles are bent outwards, is very similar to the experimental one. The interaction energy between the gold and silver fragments at this optimized distance is $-134\,kJ\,mol^{-1}$, with an ionic contribution of $-18\,kJ\,mol^{-1}$ at the HF level of theory. The slightly larger interaction distances and the presence of two weak C_{ipso}···Ag interactions instead of one for model system **C3** when compared to the experimental data is due to symmetry reasons, that is, the C_s symmetry of this model prevents the $[Ag_2(CO_2H)_2]$ fragment turning out of the plane as in the X-ray structure but allows the computational cost of this model system to be achievable.

Analysis of the interaction energy between gold and silver fragments in model **C4** leads to an Au···Ag interaction distance of 2.87 Å, very close to the experimental value of 2.88 Å. In this case the stabilization energy produced by only these two Au···Ag interactions is $-115\,kJ\,mol^{-1}$, with an attractive ionic contribution of $-17\,kJ\,mol^{-1}$ at the HF level of theory (Figure 10).

The interaction distances and stabilization energies for models **C1**–**C4** are summarized in Table 6. As mentioned above, model **C2** represents the Au···Ag interaction observed experimentally for the molecular fragment in which one $[Au(C_6F_5)(CH_2PPh_3)]$ molecule interacts with a silver center of a $[Ag_2(CO_2CF_3)_2]$ fragment. The interaction between the same fragments but through two Au···Ag interactions and one C_{ipso}···Ag interaction would be intermediate between models **C3** and **C4**. Previous ab initio studies for unsupported Au···Ag interactions also show attraction when correlation effects are included. Previously, some of us reported the metallophilic interaction between anionic gold(I) and silver(I) fragments in a square pyramidal $AuAg_4$ arrangement.[30] In this case four metallophilic Au···Ag interactions ($-13\,kJ\,mol^{-1}$ each) were attractive at the MP2 level of theory but repulsive at the HF level, due to repulsion between anionic fragments, and led to a disperse nature for the metallophilicity. Similarly, Pyykkö and co-workers showed that neutral $ClAuPH_3$ and $ClAgPH_3$ fragments have a metallophilic interaction of about $-24\,kJ\,mol^{-1}$ that arises from dispersion forces (van der Waals), since at the HF level repulsion between fragments is obtained.[31] According to study on models **C1**–**C4**, large stabilization energies are observed for each Au···Ag interaction (ca. $-60\,kJ\,mol^{-1}$) and even some ionic contribution (from -5 to $-18\,kJ\,mol^{-1}$) that indicates the presence of a charge-transfer contribution to the interaction between the electron-rich $[Au(C_6F_5)(CH_2PPh_3)]$ fragment and the acidic $[Ag_2(CO_2H)_2]$. In summary, it seems likely that this new type of metallophilic attraction is stronger than those usually observed among cationic or anionic fragments (ca. 13–24 $kJ\,mol^{-1}$), but weaker than those computed between anionic and cationic fragments (ca. $-234\,kJ\,mol^{-1}$).[32] Indeed, the stabilization energy produced would be enough to observe aggregation in solution at high concentrations.

Finally, to check that the method used herein is correct, the theoretically studied model systems were validated by a

Table 6. Interaction energy (BSSE-corrected) at the HF and MP2 levels of theory for $[Au(C_6H_5)(CH_2PH_3)]\cdots[Ag_2(CO_2H)_2]$ model systems **C1**–**C4** and for the experimental arrangement (**Exp**).

Model	R(Ag···C_{ipso})[a]	R(Au···Ag)[a]	ΔE_{int}(HF)[b]	ΔE_{int}(MP2)[b]
Exp	2.64	2.90, 2.88, 2.87	−1.7	−183
C1	2.48	2.86	−24	−98
C2	–	2.81	−5	−61
C3	2.83	3.09	−18	−134
C4	–	2.87	−17	−115

[a] Distance in angstroms. [b] Interaction energies in kilojoules per mole.

© 2009 Wiley-VCH Verlag GmbH & Co. KGaA, Weinheim

single-point MP2 calculation (BSSE-corrected) on the molecular fragment $[AuAg_4(C_6F_5)(CF_3CO_2)_4(CH_2PPh_3)]$, taking the coordinates obtained in the X-ray crystal structure. This molecular fragment includes the analysis of all the interactions at the same time, that is, three $Au^I\cdots Ag^I$ interactions and one $Ag^I\cdots C_{ipso}$ interaction. At the MP2 level of theory, an overall stabilization energy of $-183\ kJ\,mol^{-1}$ is observed, and the HF component is slightly attractive ($-1.7\ kJ\,mol^{-1}$) when no correlation effects are included. When these data are taken into account, the sum of the results obtained for models **C1**–**C4** is in good agreement with the model obtained from the experimental X-ray data (see Table 6).

Conclusions

Complex **2** has been prepared by reaction between the $[Au(C_6F_5)(CH_2PPh_3)]$ and $[Ag(CF_3CO_2)]$ in a 1:3 molar ratio. Its crystal structure consists of a polymeric arrangement built up through metallophilic gold···silver and silver···silver interactions together with silver···oxygen interactions. Concentrated solutions of **2** also show aggregation through metallophilic interactions. This aggregation has been detected by several techniques. EXAFS measurements on 45 mM THF solutions are consistent with the presence of metallophilic gold···silver interactions in solution. PGSE NMR measurements corroborate this trend, with the ratio between the molecular volumes of complexes **2** and **1** in the solid state being similar to that found in the 45 mM THF solutions. In addition, **2** is luminescent in solution at similar concentration, in contrast to other polymeric gold–silver compounds previously reported. The origin of the emission has been assigned to a ^{3}LMCT excited state on the basis of TDDFT calculations on a model that resembles the metallophilic arrangement found in the solid state. Finally, ab initio calculations support the existence of strong metallophilic interactions that arise from dispersion (van der Waals) with an ionic component contribution leading to $60\ kJ\,mol^{-1}$ of stabilization per gold···silver interaction.

Future ligand variations and experimental and theoretical studies on new gold–silver arrangements could be useful to gain insight into the nature and properties of gold···silver metallophilic interactions and the conditions for maintaining them in solution.

Experimental Section

Instrumentation: Infrared spectra were recorded in the range 4000–200 cm^{-1} on a Nicolet Nexus FTIR spectrometer on Nujol mulls between polyethylene sheets. C, H analyses were carried out with a Perkin–Elmer 240C microanalyzer. Mass spectra were recorded on a HP59987A electrospray instrument. ^{1}H, ^{19}F, and ^{31}P{^{1}H} NMR spectra were recorded on a Bruker ARX 300 in [D$_8$]THF solution. Chemical shifts are quoted relative to $CFCl_3$ (^{19}F, external) and 85 % H_3PO_4 (^{31}P external). UV/Vis absorption spectra were obtained on Hewlett–Packard 8453 diode-array UV/Vis spectrophotometer in THF and glassy solutions. Excitation and emission spectra were recorded with a Jobin–Yvon Horiba Fluorolog 3-22 Tau-3 spectrofluorimeter. Phosphorescence lifetime was recorded with a Fluoromax phosphorimeter accessory containing a UV xenon flash tube with a flash rate between 0.05 and 25 Hz. The lifetime data were fitted with the Jobin–Yvon software package and the Origin 6.1 program.

EXAFS spectra were recorded at the Au L_{III} edge by using a double-crystal Si(220) monochromator at Daresbury SRS on station 16.5. The solid sample was measured in transmission mode as a self-supporting pellet diluted (ca. 50 % w/w) in boron nitride. The sample dissolved in THF (0.045 M) was supported between sealed polyethylene windows and collected in fluorescence mode by using a 30-element Ge solid-state detector. Scans were collected over $k = 3$–$14\ Å^{-1}$ and averaged with EXCALIB, which was also used to convert the raw data into energy versus absorption data. EXBROOK was used to remove the background, and the EXAFS data were analyzed with EXCURV98 on the k^3-weighted raw data by using the Rehr–Albers approximation.[33] Phase shifts were derived from ab initio calculations using Hedin–Lundqvist exchange potentials and von Barth ground states and verified on experimental data of solid-state materials for which the structure is known. The statistical significance of additional shells to the fit was determined by the reduced χ^2 test, wherein the number of independent data points N_{ind} was calculated as $N_{ind} \sim (2\Delta k \Delta r)/\pi$, where Δk and Δr are the ranges in k and r space over which the data were fitted.

^{1}H PGSE measurements were carried out with the double stimulated echo pulse sequence (Double STE)[34] on a Bruker AVANCE 400 equipped with a BBI H-BB Z-GRD probe at 298 K (or 223 K in the case of low-temperature experiments) without spinning at different concentrations in [D$_8$]THF (5, 45 or 100 mM). Low-temperature experiments were performed at 223 K by using two coaxial NMR tubes with an air-filled space between them to avoid the problem of convection currents, which may cause a gradient-dependent line-shape distortion that would result in nonlinear plots of $\ln(I/I_0)$ versus G^2.[35]

General comments: Precursor complex $[Au(C_6F_5)(CH_2PPh_3)]$ was synthesized according to a literature procedure.[36] Silver trifluoroacetate is commercially available and was purchased from Sigma-Aldrich. THF and glassy solutions for photophysics were distilled and degassed before use.

$[AuAg_3(C_6F_5)(CF_3CO_2)_3(CH_2PPh_3)]_n$ (2): $[Ag(CF_3CO_2)]$ (0.132 g, 0.6 mmol) was added to a colorless solution of $[Au(C_6F_5)(CH_2PPh_3)]$ (0.128 g, 0.2 mmol) in dichloromethane (20 mL). The solution rapidly turned yellow. After 30 min of stirring at room temperature, the yellow solution was concentrated in vacuum to about 5 mL. Addition of *n*-hexane (10 mL) led to precipitation of **2** as an orange solid. Yield: 0.547 g (70.1 %). ^{1}H NMR (75.5 MHz, [D$_8$]THF, ppm): $\delta = 2.03$ (d, 2H, CH_2, $^2J(H,P) = 13.4$ Hz) and 8.00–7.65 (m, 15H, aromatic protons); ^{19}F NMR (282.4 MHz, [D$_8$]THF, ppm): $\delta = -116.6$ (m, 2F, F_o), -164.4 (t, 1F, F_p, $^3J(F_p,F_m) = 19.9$ Hz), -165.9 (m, 2F, F_m), -74.6 (s, 9F, CF_3CO_2); ^{31}P{^{1}H} NMR (121 MHz, [D$_8$]THF, ppm): $\delta = 31.7$ (s, PPh_3); MS (ES−): $m/z = 773$ ($[Ag_3(CF_3CO_2)_4]^-$, 100 %), (ES+): $m/z = 750$ ($[Au(CH_2Ph_3)_2]^+$, 100 %); FTIR (Nujol): $\nu(C_6F_5)$ at 1501, 961, and 790 cm^{-1}, ν(AuC) at 580 cm^{-1}, and $\nu(CF_3CO_2)$ at 1640 and 1190 cm^{-1}; elemental analysis (%) calcd for $C_{31}H_{17}Ag_3AuF_{14}O_6P$: C 28.57, H 1.31; found: C 28.38, H 1.52.

Crystallography: Crystals were mounted in inert oil on glass fibers and transferred to the cold gas stream of a Nonius Kappa CCD area-detector diffractometer equipped with an Oxford Instruments low-temperature attachment. Data were collected with graphite-monochromated $Mo_{K\alpha}$ radiation ($\lambda = 0.71073$ Å), scan type ω and ϕ. Absorption corrections: numerical (based on multiple scans). The structures were solved by direct methods and refined on F^2 with the program SHELXL-97.[37] All non-hydrogen atoms were anisotropically refined and hydrogen atoms were included by using a riding model. Further details on the data collection and refinement methods can be found in Table 1. CCDC 712220 (**1**) and 712221 (**2**) contain the supplementary crystallographic data for this paper. These data can be obtained free of charge from The Cambridge Crystallographic Data Centre via www.ccdc.cam.ac.uk/data_request/cif.

Theoretical methods: All calculations were performed with the Gaussian 03 program package.[38] The molecular geometries of model systems $[Au(C_6H_5)(CH_2PH_3)]$ (**A**) and $[Ag_2(CO_2H)_2]$ (**B**) were initially optimized at the DFT level of theory with the B3LYP functional. The model system $[Au(C_6H_5)(CH_2PH_3)]\cdots[Ag_2(CO_2H)_2]$ (**C1**), which represents the molecu-

 © 2009 Wiley-VCH Verlag GmbH & Co. KGaA, Weinheim

lar structure in which a $[Ag_2(CO_2H)_2]$ fragment interacts with a Au^I fragment through only one Au···Ag interaction, was built up from the separate fragments **A** and **B**. Model system $[Au(C_6H_5)(CH_2PH_3)]$···$[Ag_2(CO_2H)_2]$ (**C2**) is similar to **C1** but displays one Au^I···Ag^I interaction and one Ag···C_{ipso} interaction at the same time, and it was optimized at the B3LYP DFT level of theory in C_s symmetry. Model $[Au(C_6H_5)(CH_2PH_3)]$···$[Ag_2(CO_2H)_2]$ (**C3**), which represents the molecular fragment in which two Au^I···Ag^I interactions and two Ag···C_{ipso} interactions are present, was optimized at the MP2 level of theory in C_s symmetry. In this case the DFT level of theory does not optimize the silver fragment with bent O-Ag-O angles as in the experimental structure. Finally, model $[Au(C_6H_5)(CH_2PH_3)]$···$[Ag_2(CO_2H)_2]$ (**C4**) was built up by displacement of the Au^I fragment in order to avoid Ag···C_{ipso} interactions and analyze only the two metallophilic Au···Ag interactions in C_s symmetry (see Figure 8). Electronic correlation effects, keeping the core orbitals frozen, were included in further single-point calculations at various Au···Ag distances or Ag···C_{ipso} distances by using second-order Møller–Plesset perturbation theory or Hartree–Fock calculations on model systems **C1**–**C4**. These models were chosen to represent the experimental geometry of polymeric complex **2** by substituting the C_6F_5 rings in X-ray diffraction structure by C_6H_5 rings, the Ph groups of the ylide ligand by H atoms, and the trifluoroacetate ligands by formate ligands, to reduce the computational cost.

For TDDFT calculations, the molecular structures of $[Au(C_6F_5)(CH_2PPh_3)]$ and $[AuAg_4(C_6F_5)(CF_3CO_2)_4(CH_2PPh_3)]_n$ were taken from the X-ray diffraction data for complexes **1** and **2**, respectively. Keeping all distances, angles, and dihedral angles frozen, single-point DFT calculations were performed on the models. In the single-point ground-state calculations and subsequent calculations of the electronic excitation spectra, the B3LYP functional[39] as implemented in TURBOMOLE[40] was used (see Supporting Information for details).

Acknowledgements

This work was supported by the DGI(MEC)/FEDER (CTQ2007-67273-C02-02). R.C.P. and E.S.-F. thank M.E.C. and JAE-CSIC for grants and the authors thank Mohammad Omary for helpful comments. CCLRC are thanked for EXAFS beam time.

[1] C. Janiak, *Dalton Trans.* **2003**, 2781.
[2] D. Maspoch, D. Ruiz-Molina, J. Veciana, *Chem. Soc. Rev.* **2007**, *36*, 770.
[3] P. Pyykkö, *Chem. Rev.* **1997**, *97*, 597.
[4] P. Pyykkö, *Angew. Chem.* **2004**, *116*, 4512; *Angew. Chem. Int. Ed.* **2004**, *43*, 4412.
[5] P. Pyykkö, *Inorg. Chim. Acta* **2005**, *358*, 4113.
[6] a) P. Pyykkö, *Chem. Soc. Rev.* **2008**, *37*, 1967; b) H. Schmidbaur, A. Schier, *Chem. Soc. Rev.* **2008**, *37*, 1931.
[7] See for example: a) H. H. Karsch, U. Schubert, *Z. Naturforsch. B* **1982**, *37*, 186; b) T. Tsuda, S. Ohba, M. Takahashi, M. Ito, *Acta Crystallogr. Sect. C* **1989**, *45*, 887; c) M. Jansen, *Angew. Chem.* **1987**, *99*, 1136; *Angew. Chem. Int. Ed. Engl.* **1987**, *26*, 1098.
[8] A. Heine, R. Herbst-Irmer, D. Stalke, *J. Chem. Soc. Chem. Commun.* **1993**, 1729.
[9] H. Schmidbaur, H.-J. Öller, D. L. Wilkinson, B. Huber, G. Müller, *Chem. Ber.* **1989**, *122*, 31.
[10] S. Otsuka, *J. Organomet. Chem.* **1980**, *200*, 191.
[11] Y.-L. Pan, J. T. Mage, M. J. Fink, *J. Am. Chem. Soc.* **1993**, *115*, 3842.
[12] See for example: a) R. Blom, H. Werner, J. Wolf, *J. Organomet. Chem.* **1988**, *354*, 293; b) H. Pritzkow, P. Jennische, *Acta Chem. Scand.* **1975**, *29*, 60; c) B. Krebs, H. Greiwing, *Z. Anorg. Allg. Chem.* **1992**, *616*, 145.
[13] L. A. Bengtsson, R. Hoffmann, *J. Am. Chem. Soc.* **1993**, *115*, 2666.
[14] See for example: a) J. K. Nagle, A. L. Balch, M. M. Olmstead, *J. Am. Chem. Soc.* **1988**, *110*, 319; b) A. L. Balch, B. J. Davis, E. Y. Fung, M. M. Olmstead, *Inorg. Chim. Acta* **1993**, *212*, 149; c) A. L. Balch, J. K. Nagle, M. M. Olmstead, P. E. Reedy, Jr., *J. Am. Chem. Soc.* **1987**, *109*, 4123; d) S. Wang, J. P. Fackler, Jr., C. King, J. C. Wang, *J. Am. Chem. Soc.* **1988**, *110*, 3308; e) S. Wang, G. Garzón, C. King, J. C. Wang, J. P. Fackler, Jr., *Inorg. Chem.* **1989**, *28*, 4623; f) J. C. Jeffery, P. A. Jelliss, F. G. A. Stone, *Inorg. Chem.* **1993**, *32*, 3943; g) T. F. Carlson, J. P. Fackler, Jr., R. J. Staples, R. E. P. Winpenny, *Inorg. Chem.* **1995**, *34*, 426; h) H.-K. Yip, H.-M. Lin, Y. Wang, C.-M. Che, *J. Chem. Soc. Dalton Trans.* **1993**, 2939; i) O. Crespo, A. Laguna, E. J. Fernández, J. M. López-de-Luzuriaga, P. G. Jones, M. Teichert, M. Monge, P. Pyykkö, N. Runeberg, M. Schütz, H.-J. Werner, *Inorg. Chem.* **2000**, *39*, 4786.
[15] a) C. K. Chang, C. X. Guo, K. K. Cheung, D. Li, C.-M. Che, *J. Chem. Soc. Dalton Trans.* **1994**, 3677; b) H. de La Riva, M. Nieuwhuyzen, C. M. Fierro, P. R. Raithby, L. Male, M. C. Lagunas, *Inorg. Chem.* **2006**, *45*, 1418; c) E. J. Fernández, A. Laguna, J. M. López-de-Luzuriaga, M. Monge, M. Montiel, M. E. Olmos, *Inorg. Chem.* **2005**, *44*, 1163; d) E. J. Fernández, A. Laguna, J. M. López-de-Luzuriaga, M. Monge, M. Montiel, M. E. Olmos, M. Rodríguez-Castillo, *Organometallics* **2006**, *25*, 3639.
[16] a) R. Usón, A. Laguna, M. Laguna, P. G. Jones, G. M. Sheldrick, *J. Chem. Soc. Chem. Commun.* **1981**, 1097; b) R. Usón, A. Laguna, M. Laguna, P. G. Jones, G. M. Sheldrick, *J. Chem. Soc. Dalton Trans.* **1984**, 285; c) A. Burini, A. R. Bravi, J. P. Fackler, Jr., R. Galassi, T. A. Grant, M. A. Omary, B. R. Pietroni, R. J. Staples, *Inorg. Chem.* **2000**, *39*, 3158; d) A. Burini, J. P. Fackler, Jr., R. Galassi, B. R. Pietroni, R. J. Staples, *Chem. Commun.* **1998**, 95; e) M. Contel, J. Garrido, M. C. Gimeno, M. Laguna, *J. Chem. Soc. Dalton Trans.* **1998**, 1083; f) R. Usón, A. Laguna, M. Laguna, A. Usón, P. G. Jones, C. F. Erdbrugger, *Organometallics* **1987**, *6*, 1778; g) O. Schuster, U. Monkowius, H. Schmidbaur, R. S. Ray, S. Krüger, N. Rösch, *Organometallics* **2006**, *25*, 1004; h) E. J. Fernández, P. G. Jones, A. Laguna, J. M. López-de-Luzuriaga, M. Monge, M. E. Olmos, R. C. Puelles, *Organometallics* **2007**, *26*, 5931; i) E. J. Fernández, J. M. López-de-Luzuriaga, M. Monge, M. E. Olmos, R. C. Puelles, A. Laguna, A. A. Mohamed, J. P. Fackler, Jr., *Inorg. Chem.* **2008**, *47*, 8069; j) E. J. Fernández, J. M. López-de-Luzuriaga, A. Laguna, *Dalton Trans.* **2007**, 1969.
[17] D. Perreault, M. Drouin, A. Michel, V. M. Miskowski, W. P. Schaefer, P. D. Harvey, *Inorg. Chem.* **1992**, *31*, 695.
[18] J. M. López-de-Luzuriaga in *Modern Supramolecular Gold Chemistry* (Ed.: A. Laguna), Wiley-VCH, Weinheim, **2008**, pp. 347–398, and references therein.
[19] See for example: a) H. Schmidbaur, *Gold Bull.* **2000**, *33*, 3; b) J. Vicente, M. T. Chicote, I. Saura-Llamas, M. C. Lagunas, M. C. Ramírez de Arellano, P. González-Herrero, M. D. Abrisqueta, R. Guerrero in *Metal Clusters in Chemistry, Vol. 1* (Eds.: P. Braunstein, L. Oro, P. R. Raithby), Wiley-VCH, Weinheim, **1999**, pp. 493–508; c) J. C. Vickery, M. M. Olmstead, E. Y. Fung, A. L. Balch, *Angew. Chem.* **1997**, *112*, 1227; *Angew. Chem. Int. Ed. Engl.* **1997**, *36*, 1179; d) B. C. Tzeng, C. K. Chang, K. K. Cheung, C.-M. Che, S. M. Peng, *Chem. Commun.* **1997**, 135; e) Z. Assefa, B. G. McBurnett, R. J. Staples, J. P. Fackler, Jr., B. Assmann, K. Angermaier, H. Schmidbaur, *Inorg. Chem.* **1995**, *34*, 75; f) Z. Assefa, B. G. McBurnett, B. G. Staples, R. J. Fackler, Jr., *Inorg. Chem.* **1995**, *34*, 4965; g) C.-M. Che, H.-L. Kwong, C.-K. Poon, V. W.-W. Yam, *J. Chem. Soc. Dalton Trans.* **1990**, 3215; h) R. Narayanaswamy, M. A. Young, E. Parkhurst, M. Ouellette, M. E. Kerr, D. M. Ho, R. C. Elder, A. E. Bruce, M. R. M. Bruce, *Inorg. Chem.* **1993**, *32*, 2506.
[20] A. Burini, J. P. Fackler, Jr., R. Galassi, A. Macchioni, M. A. Omary, M. A. Rawashdeh-Omary, B. R. Pietroni, S. Sabatini, C. Zuccaccia, *J. Am. Chem. Soc.* **2002**, *124*, 4570.
[21] H. de La Riva, A. Pintado-Alba, M. Nieuwenhuyzen, C. Hardacre, M. C. Lagunas, *Chem. Commun.* **2005**, 4970.
[22] H. Schmidbaur, R. Franke, *Inorg. Chim. Acta* **1975**, *13*, 85.
[23] a) R. Usón, A. Laguna, M. Laguna, B. R. Manzano, P. G. Jones, G. M. Sheldrick, *J. Chem. Soc. Dalton Trans.* **1984**, 839; b) R. Usón, A. Laguna, M. Laguna, M. C. Gimeno, P. G. Jones, G. M. Sheldrick, *Chem. Commun.* **1996**, 509; c) M. C. Gimeno, A. Laguna, F. Sanmartín, P. G. Jones, *Organometallics* **1993**, *12*, 3984; d) R. Usón, A.

 © 2009 Wiley-VCH Verlag GmbH & Co. KGaA, Weinheim

Laguna, M. Laguna, I. Lázaro, P. G. Jones, *Organometallics* **1987**, *6*, 2326; e) R. Usón, A. Laguna, M. Laguna, I. Lázaro, A. Morata, P. G. Jones, G. M. Sheldrick, *Chem. Soc. Dalton Trans.* **1986**, 669; f) R. Usón, A. Laguna, M. Laguna, M. N. Fraile, I. Lázaro, M. C. Gimeno, P. G. Jones, C. Reihs, G. M. Sheldrick, *J. Chem. Soc. Dalton Trans.* **1990**, 333; g) M. C. Gimeno, P. G. Jones, A. Laguna, M. Laguna, I. Lázaro, *J. Chem. Soc. Dalton Trans.* **1993**, 2223.

[24] a) E. Cerrada, M. C. Gimeno, A. Laguna, M. Laguna, V. Orera, P. G. Jones, *J. Organomet. Chem.* **1996**, *506*, 203; b) J. Vicente, A. R. Singhal, P. G. Jones, *Organometallics* **2002**, *21*, 5887.

[25] A. Bayler, A. Schier, G. A. Bowmaker, H. Schmidbaur, *J. Am. Chem. Soc.* **1996**, *118*, 7006; b) M. C. Blanco, E. J. Fernández, P. G. Jones, A. Laguna, J. M. López-de-Luzuriaga, M. E. Olmos, *Angew. Chem.* **1998**, *110*, 3199; *Angew. Chem. Int. Ed.* **1998**, *37*, 3042.

[26] E. J. Fernández, A. Laguna, J. M. López-de-Luzuriaga, M. Montiel, M. E. Olmos, J. Pérez, R. C. Puelles, *Organometallics* **2006**, *25*, 4307.

[27] a) J. Powell, M. J. Horvath, A. Lough, A. Phillips, J. Brunet, *J. Chem. Soc. Dalton Trans.* **1998**, 637; b) C.-M. Che, M.-C. Tse, M. C. W. Chan, K.-K. Cheung, D. L. Phillips, K.-H. Leung, *J. Am. Chem. Soc.* **2000**, *122*, 2464; c) T. Tsuchiya, T. Shimizu, K. Hirabayashi, N. Kamigata, *J. Org. Chem.* **2002**, *67*, 6632; d) M. C. Brandys, R. J. Puddephatt, *J. Am. Chem. Soc.* **2002**, *124*, 3946; e) L. Brammer, M. D. Burgard, M. D. Eddleston, C. S. Rodger, N. P. Rath, H. Adams, *CrystEngComm* **2004**, *44*, 239; f) B. Djordjevic, O. Schuster, H. Schmidbaur, *Inorg. Chem.* **2005**, *44*, 673; g) J. C. Zhong, M. Munakata, M. Maekawa, T. Kuroda-Sowa, Y. Suenaga, H. Konaka, *Inorg. Chim. Acta* **2003**, *342*, 202; h) N. Schultheiss, D. R. Powell, E. Bosch, *Inorg. Chem.* **2003**, *42*, 5304; i) E. Bosch, C. L. Barnes, *Inorg. Chem.* **2002**, *41*, 2543; j) M. O. Awaleh, A. Badia, F. Brisse, X.-H. Bu, *Inorg. Chem.* **2006**, *45*, 1560.

[28] J. M. Forward, J. P. Fackler, Jr., Z. Assefa in *Optoelectronic Properties of Inorganic Compounds* (Eds.: D. M. Roundhill, J. P. Fackler, Jr.), Plenum Press, New York, **1999**, pp. 195–226.

[29] a) E. J. Fernández, M. C. Gimeno, A. Laguna, J. M. López-de-Luzuriaga, M. Monge, P. Pyykkö, D. Sundholm, *J. Am. Chem. Soc.* **2000**, *122*, 7287; b) M. A. Rawashdeh-Omary, M. A. Omary, J. P. Fackler, Jr., *Inorg. Chim. Acta* **2002**, *334*, 376; c) S. S. Tang, C.-P. Chang, I. J. B. Lin, L.-S. Liou, J.-C. Wang, *Inorg. Chem.* **1997**, *36*, 2294; d) M. A. Rawashdeh-Omary, M. A. Omary, H. H. Patterson, *J. Am. Chem. Soc.* **2000**, *122*, 10371.

[30] E. J. Fernández, A. Laguna, J. M. López-de-Luzuriaga, M. Monge, M. E. Olmos, R. C. Puelles, *J. Phys. Chem. B* **2005**, *109*, 20652.

[31] P. Pyykkö, N. Runeberg, F. Mendizabal, *Chem. Eur. J.* **1997**, *3*, 1451.

[32] E. J. Fernández, A. Laguna, J. M. López-de-Luzuriaga, M. Monge, P. Pyykkö, N. Runeberg, *Eur. J. Inorg. Chem.* **2002**, 750.

[33] N. Binstead, EXCURV98, CCLRC Daresbury Laboratory computer program, **1998**.

[34] A. A. Khrapitchev, P. T. Callaghan, *J. Magn. Reson.* **2001**, *152*, 259.

[35] E. Martínez-Viviente, P. S. Pregosin, *Helv. Chim. Acta* **2003**, *86*, 2364, and references therein.

[36] R. Usón, A. Laguna, M. Laguna, A. Usón, M. C. Gimeno, *Synth. React. Inorg. Met.-Org. Chem.* **1988**, *18*, 69.

[37] G. M. Sheldrick, University of Göttingen: Göttingen, Germany, **1997**.

[38] Gaussian 03, Revision C.02, M. J. Frisch, G. W. Trucks, H. B. Schlegel, G. E. Scuseria, M. A. Robb, J. R. Cheeseman, J. A. Montgomery, Jr., T. Vreven, K. N. Kudin, J. C. Burant, J. M. Millam, S. S. Iyengar, J. Tomasi, V. Barone, B. Mennucci, M. Cossi, G. Scalmani, N. Rega, G. A. Petersson, H. Nakatsuji, M. Hada, M. Ehara, K. Toyota, R. Fukuda, J. Hasegawa, M. Ishida, T. Nakajima, Y. Honda, O. Kitao, H. Nakai, M. Klene, X. Li, J. E. Knox, H. P. Hratchian, J. B. Cross, V. Bakken, C. Adamo, J. Jaramillo, R. Gomperts, R. E. Stratmann, O. Yazyev, A. J. Austin, R. Cammi, C. Pomelli, J. W. Ochterski, P. Y. Ayala, K. Morokuma, G. A. Voth, P. Salvador, J. J. Dannenberg, V. G. Zakrzewski, S. Dapprich, A. D. Daniels, M. C. Strain, O. Farkas, D. K. Malick, A. D. Rabuck, K. Raghavachari, J. B. Foresman, J. V. Ortiz, Q. Cui, A. G. Baboul, S. Clifford, J. Cioslowski, B. B. Stefanov, G. Liu, A. Liashenko, P. Piskorz, I. Komaromi, R. L. Martin, D. J. Fox, T. Keith, M. A. Al-Laham, C. Y. Peng, A. Nanayakkara, M. Challacombe, P. M. W. Gill, B. Johnson, W. Chen, M. W. Wong, C. Gonzalez, J. A. Pople, Gaussian, Inc., Wallingford, CT, **2004**.

[39] a) A. D. Becke, *J. Chem. Phys.* **1992**, *96*, 2155; b) A. D. Becke, *J. Chem. Phys.* **1993**, *98*, 5648; c) C. Lee, W. Yang, R. G. Parr, *Phys. Rev. Lett.* **1998**, *37*, 785.

[40] R. Ahlrichs, M. Bär, M. Häser, H. Horn, C. Kölmel, *Chem. Phys. Lett.* **1989**, *162*, 165.

Received: January 20, 2009
Published online: May 13, 2009

 © 2009 Wiley-VCH Verlag GmbH & Co. KGaA, Weinheim